

## Porosity induced magnetic granularity in epitaxial $\text{YBa}_2\text{Cu}_3\text{O}_7$ thin films

A. Pomar, J. Gutiérrez, A. Palau,\* T. Puig, and X. Obradors

*Institut de Ciència de Materials de Barcelona – CSIC, Campus de la UAB, 08193 Bellaterra, Spain*

(Received 18 April 2006; published 23 June 2006)

We present a study of the interrelation between porosity and magnetic granularity in epitaxial  $\text{YBa}_2\text{Cu}_3\text{O}_7$  thin films. The main signature of the magnetic granularity is the shift in the hysteresis loops of the maximum magnetization to positive applied magnetic fields. The existing pores promote the formation of constrictions where the capability to carry current is reduced and the sample behaves as a granular material with two critical current densities, a local  $J_c^G$  and a percolating  $J_c^{\text{PERC}}$ . We show that only  $J_c^{\text{PERC}}$  depends on porosity and it exhibits a clear correlation with normal state resistivity. On its side,  $J_c^G$  reflects the local current density of the films and it is not modified by the presence of holes. The geometrical origin of the magnetic granularity is confirmed by observing the same phenomenology in thin films where porosity has been artificially induced.

DOI: [10.1103/PhysRevB.73.214522](https://doi.org/10.1103/PhysRevB.73.214522)

PACS number(s): 74.25.Ha, 74.25.Sv, 74.72.Bk, 74.81.Bd

The study of granularity effects in high temperature superconductors has gained a renewed interest in these last years. This is mainly due to the fact that the most promising material candidates for power applications,  $\text{YBa}_2\text{Cu}_3\text{O}_7$  (YBCO) coated conductors (CCs), usually exhibit granular behavior.<sup>1</sup> Therefore, the capability to carry current is controlled by the interplay between two critical current densities: an intragrain  $J_c^G$ , mainly governed by the vortex pinning properties of the YBCO grains and an intergrain  $J_c^{\text{PERC}}$ , which is determined by the characteristics of the low-angle grain boundaries (GBs) network.<sup>1,2</sup> To understand such interplay many efforts have been done mainly aiming to get independent information on both quantities.<sup>3–7</sup> These approaches are based either on destructive experimental techniques or they are well suited if the intergrain current is significantly lower than the intragrain current. This latter is not the usual situation for good quality CCs where  $J_c^G$  and  $J_c^{\text{PERC}}$  can be comparable. For this case, a unique methodology based on dc inductive measurements has been recently developed which allows the simultaneous determination of  $J_c^G$  and  $J_c^{\text{PERC}}$  (Ref. 8) from a detailed analysis of minor magnetic hysteresis loops. The main experimental feature is a shift of the maximum magnetization towards positive applied fields due to the trapped field in the grains returning through the GBs. This technique has already been applied to several critical issues in CCs.<sup>8–11</sup>

On the other hand, *ex situ* chemical solution deposition based techniques and, in particular the trifluoroacetates (TFA) route are leading the race of low-cost deposition methods to prepare high-quality YBCO CCs.<sup>12,13</sup> To improve the superconducting properties of epitaxial TFA-YBCO films many studies have been focused towards the understanding of the influence of microstructural features on the critical current density  $J_c$ .<sup>14–16</sup> Due to their typical island mode growth, the volume reduction generated when secondary phases are converted to YBCO leads to the trapping of holes inside the *c*-axis YBCO matrix.<sup>14</sup> Thus, unless processing conditions are finely optimized, TFA-YBCO films exhibit significant residual porosity which is then the limiting factor of the engineering critical current.<sup>13–18</sup> Also, it has been reported by other authors that artificial constrictions can lead to a granular behavior in superconducting thin films.<sup>19–21</sup> Here

we present a detailed study of a similar effect of magnetic granularity in samples with different degrees of porosity. In previous works we have demonstrated an universal correlation between critical current density and normal state resistivity.<sup>13,16–18</sup> The present new experimental results allow us to clarify the origin of this correlation and to establish that indeed porosity is controlling the current percolating over the whole sample whereas the local critical current is determined by vortex pinning and remains unchanged. This study is then a powerful tool to track the improvements in  $J_c^G$  and  $J_c^{\text{PERC}}$  when optimizing the different processing parameters. This phenomenology keeps some similarity to the behavior recently described for single crystalline superconducting foams.<sup>22</sup> We will confirm the geometrical origin of this granularity by observing the same phenomenology in a sample with porosity artificially generated by photolithography.

The samples here studied are *c*-axis oriented epitaxial YBCO thin films grown on  $\text{LaAlO}_3$  single crystalline substrates by the trifluoroacetates route following a three step (pyrolysis, growth, and oxygenation) procedure described before.<sup>13,18,23,24</sup> Although a detailed discussion of the influence of processing parameters on the final residual porosity of the films is beyond the scope of this work we should address that, in the present case, variations in porosity arise mainly from the different pyrolysis profiles used for each sample.<sup>13</sup> Reaction conditions were kept unchanged and they were chosen (795 °C,  $\text{PH}_2\text{O}=7$  mbar,  $\text{PO}_2=0.2$  mbar) to minimize the nucleation of *a*-axis oriented YBCO grains which also have a strong influence in porosity.<sup>16</sup> Films are 300 nm thick and their microstructure was characterized by x-ray diffraction and by scanning electron microscopy (SEM). Normal state resistivity  $\rho_{300\text{ K}}$  was measured by a standard nondestructive four-point contact technique. Minor magnetic hysteresis loops (MHLs) were performed at 5 K after a zero-field cooling process in a commercial dc SQUID magnetometer provided with a 7 T superconducting magnet. Magnetization was measured in the forward and reversal branches of  $M(H)$  loops with maximum applied field  $H_{\text{max}}$  progressively increased until saturation was reached. Transport critical current densities were determined on a microbridge 20  $\mu\text{m}$  wide and 2 mm long with the usual criterion

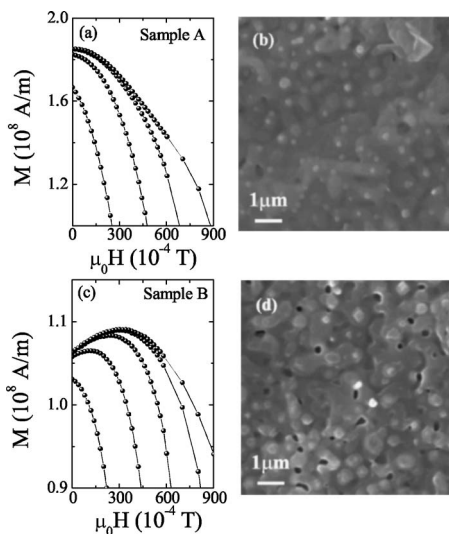


FIG. 1. Details of the reversal branches of minor magnetic hysteresis loops at 5 K for a porous free (a) and a porous (c) TFA-YBCO thin film. The maximum applied magnetic fields for the loops are 0.06, 0.08, 0.1, and 0.12 T in (a) and 0.06, 0.08, 0.1, 0.12, and 0.14 T in (c). SEM images at the surface of both samples evidencing the absence or presence of pores are shown in (b) and (d), respectively.

of  $1 \mu\text{V}/\text{cm}$ . In all the experiments the magnetic field  $H_a$  has been applied along the  $c$  axis.

The typical magnetic behavior observed from the MHLs of TFA-YBCO thin films with different degrees of porosity are summarized in Fig. 1. First, in Fig. 1(a) we present the results obtained for a fully densified YBCO film, sample A. A SEM image of the surface of this sample revealing the absence of pores is also shown in Fig. 1(b). In this case we can observe that the MHLs always exhibit a peak centered at  $H_a=0$ . This peak position remains unchanged when increasing the maximum magnetic field of the MHL and it is still zero when saturation is reached for  $\mu_0 H_{\text{max}} \geq 0.12$  T. This behavior is the expected one for a superconducting thin film with large demagnetization effects and a field dependent  $J_c$  and it has been previously reported for *in situ* YBCO thin films.<sup>8,25</sup> On the other hand, a different magnetic behavior has been found when residual porosity remains in the sample. This is exemplified in Fig. 1(c) for sample B that exhibits the porosity illustrated in the SEM image of Fig. 1(d). In this case the maximum magnetization  $M_{\text{max}}$  is not always achieved at  $H_a=0$  but instead the peak position  $H_{\text{peak}}$  increases as  $H_{\text{max}}$  is increased until it achieves a saturation position  $H_{\text{peak}}^{\text{sat}}$  for a given  $H_{\text{max}}^{\text{sat}}$  value. This different evolution of the MHLs for samples A and B in Figs. 1(a) and 1(c) above described has been summarized in Fig. 2. Here we represent the peak position as a function of  $H_{\text{max}}$  in the different MHL for both samples. A similar behavior of the hysteresis loops with  $M_{\text{max}}$  achieved at  $H_a > 0$  has been previously observed in several superconducting systems such as BSCCO tapes,<sup>26</sup> YBCO coated conductors,<sup>8</sup> and artificially granular thin films.<sup>19–21</sup> In all those works the peak at  $H_a > 0$  has been ascribed to granularity. The mechanism for peak shift is the following: In the reversal branch of the MHL, the local magnetic field at the grain boundaries  $H_{\text{loc}}^{\text{GB}}$  is

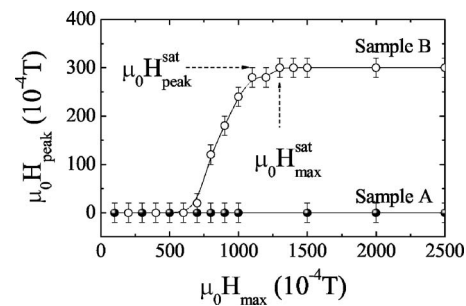


FIG. 2. Evolution of the peak position in the hysteresis loops of Fig. 1(a) and 1(d) as a function of maximum applied field. Arrows indicate the values of  $\mu_0 H_{\text{peak}}^{\text{sat}}$  and  $\mu_0 H_{\text{max}}^{\text{sat}}$  taken for sample B and used in the equations to evaluate  $J_c^G$  for this sample.

the sum of the applied field and the return field  $H_{\text{return}}$  through the GBs resulting from the flux lines trapped into the superconducting grains. Thus, a maximum in the magnetization will occur when  $H_{\text{loc}}^{\text{GB}} \sim 0$ . As the loops reflect the behavior of the intragrain contribution the peak is shifted to positive fields.<sup>8</sup> Its position depends on the value of  $H_{\text{return}}$  and it will increase with  $H_{\text{max}}$  until saturation of the grain magnetization is reached in which case  $H_{\text{return}}$  (and therefore  $H_{\text{peak}}$ ) will be no longer dependent of  $H_{\text{max}}$ . However our samples are epitaxial YBCO thin films with an average in-plane misorientation of less than  $1^\circ$  as characterized by the full width at half maximum of the  $\phi$  scan of the (102) reflection. Thus, these granularity effects are not expected to arise from the presence of low angle GBs network<sup>27</sup> but, instead, it should have their origin in their main microstructural feature, i.e., the different degrees of porosity. As it can be seen from Fig. 1(d), the presence of pores leads to the creation of constrictions and even if the local  $J_c$  is not changed, the capability to carry current is reduced by such constrictions. We can assume then that magnetic grains are formed between the holes and magnetic flux can remain trapped in these grains and return through the network of holes or constrictions. The material behaves as a granular system with two critical current densities, an intragrain  $J_c^G$  and a percolating  $J_c^{\text{PERC}}$ , even in absence of GBs in the sample. A similar development due to porosity of a system with two critical currents but without GBs has been previously observed in single crystalline superconducting foams.<sup>22</sup>

As it has been stressed before, in the last years our group has developed a methodology to study granularity effects from systematic measurements of the MHLs which allows us to independently determine both the intragrain  $J_c^G$  and the intergrain  $J_c^{\text{PERC}}$  critical current densities.<sup>8</sup> Although a detailed description of this methodology can be found elsewhere<sup>8</sup> it is worth noting that  $J_c^{\text{PERC}}$  is obtained from the magnetization value at the saturated peak through the expression,  $J_c^{\text{PERC}} = 3M_{\text{peak}}^{\text{sat}}/R$  with  $R$  being the sample radius. On the other hand, by assuming that  $H_{\text{return}}$  through a single GB arise from the contribution of two isolated adjacent cylindrical grains,  $J_c^G$  and the average magnetic grain size  $\langle 2a \rangle$  can be determined by simultaneously solving the equations

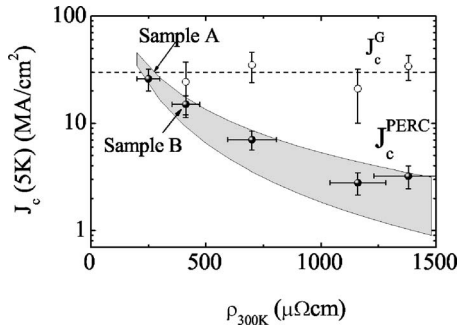


FIG. 3. Dependence of the local  $J_c^G$  and of the percolating  $J_c^{\text{PERC}}$  critical current densities at 5 K for a series of TFA-YBCO thin films as a function of normal state resistivity  $\rho_{300\text{ K}}$ . The  $J_c^G$  and  $J_c^{\text{PERC}}$  values have been obtained from the analysis of the MHLs as indicated in the main text. The values for samples *A* and *B* are also indicated. The previously reported correlation between  $\rho_{300\text{ K}}$  and  $J_c^{\text{PERC}}$  for a large number of TFA-YBCO samples is plotted as a shadowed region.

$$\frac{H_{\text{peak}}^{\text{sat}}}{H_{\text{max}}^{\text{sat}}} = g(a/L) \quad \text{and} \quad J_c^G = \frac{H_{\text{peak}}^{\text{sat}}}{Lx(a/L)}, \quad (1)$$

where  $H_{\text{peak}}^{\text{sat}}$  and  $H_{\text{max}}^{\text{sat}}$  are experimental values obtained as indicated in Fig. 2 and  $g$  and  $x$  are dimensionless factors which depends on  $a/L$ ,  $L$  being the sample thickness.<sup>8</sup> We proceed to apply this methodology to a series of TFA-YBCO thin films with different porosities.

One of the main problems to quantitatively study the influence of porosity in the properties of any material is that in many cases, as for example to evaluate the electrical conductivity of a two-dimensional (2D) system with holes,<sup>28</sup> the total hole fraction is not the right parameter and a precise knowledge of the detailed shape and distribution of the pores is needed. This information is usually inaccessible and other methodologies should be taken into consideration. For TFA-YBCO thin films we have recently shown that the electrical resistivity at room temperature has a strong correlation with the porosity observed from SEM images and it can be used as a quantifying parameter. With this idea in mind we have plotted in Fig. 3 the results of our magnetometry analysis, i.e.,  $J_c^G$  and  $J_c^{\text{PERC}}$  values obtained for each sample as a function of  $\rho_{300\text{ K}}$  and, for clarity, we have also indicated the values corresponding to samples *A* and *B*.  $J_c^{\text{PERC}}$  may decrease by one order of magnitude while  $J_c^G$  remains constant within 30% dispersion. This confirms the geometrical mechanisms above proposed to explain the anomalous behavior of the MHLs as  $J_c^G$  indeed reflects the local critical current density in the samples and it is expected to be mainly determined by vortex pinning mechanisms and not by geometrical factors. Another important fact is a stronger dependence of  $J_c^{\text{PERC}}$  on porosity (factor of 10) than that of  $\rho_{300\text{ K}}$  (factor of 4–5). This fact, that it has been pointed out before,<sup>29</sup> just reflects that the effect of a constriction in the current flow is more dramatic in a highly nonlinear system as a superconductor than in a linear, ohmic behavior. This general correlation between  $\rho_{300\text{ K}}$  and  $J_c^{\text{PERC}}$  has been also plotted as a shadowed region in Fig. 3, representative of a large

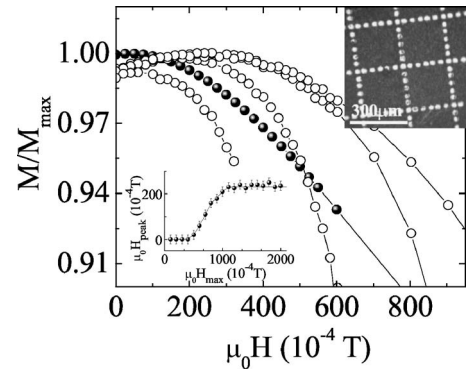


FIG. 4. Reversal branches of the hysteresis loops before (closed symbols,  $\mu_0 H_{\text{max}} = 0.2\text{ T}$ ) and after (open symbols,  $\mu_0 H_{\text{max}} = 0.06, 0.08, 0.11,$  and  $0.14\text{ T}$ ) the generation of artificial porosity in a YBCO PLD thin film by patterning the sample as shown in the optical picture (upper inset). The lower inset shows the evolution of the peak position after patterning as a function of the maximum applied field.

number of YBCO thin films ( $\sim 150$  samples). Although some differences could be expected as a function of porosity, our results gave an average magnetic grain size of  $\langle 2a \rangle \sim 1.0\ \mu\text{m} \pm 0.3\ \mu\text{m}$  without any clear correlation with  $\rho_{300\text{ K}}$ . Further investigations are needed to clarify if these  $\langle 2a \rangle$  values can be somehow related to the typical island growth mode observed in the TFA route. It is worth noting that  $J_c^G$  represents also the target value to be achieved when all the processing parameters in TFA-YBCO growth are optimized to minimize porosity.

To validate the above scenario we have checked whether artificially generated porosity is able to raise granularity effects as those observed in Fig. 1. For that experiment we have taken a fully-densified YBCO thin film grown by pulsed laser deposition with  $J_c = 2.5 \times 10^7\text{ A/cm}^2$  at 5 K. As it is expected, no anomalies are observed in the MHLs as shown in the saturated loop,  $\mu_0 H_{\text{max}} = 0.2\text{ T}$  of Fig. 4 (solid symbols). Afterwards, we have fabricated an artificial porous film by patterning the sample as illustrated in the image of Fig. 4. Holes of  $30 \pm 5\ \mu\text{m}$  diameter spaced by constrictions  $10 \pm 5\ \mu\text{m}$  wide have been generated to define a bidimensional array of  $220\ \mu\text{m} \times 220\ \mu\text{m}$  squares. This particular geometry has been chosen because simulations of its critical state with the software “Trazacorrientes”<sup>29</sup> indicate that it should lead to a granular system with a ratio between percolating and grain critical currents of  $J_c^{\text{PERC}}/J_c^G \sim 0.25$ . After patterning, its magnetic behavior was measured again, the results being the open symbols in Fig. 4. We clearly observe the development of a magnetization peak at positive applied magnetic fields. Furthermore, the behavior of this peak as a function of  $H_{\text{max}}$  fully reproduces the previously described (see inset of Fig. 4). We have determined that, after lithography,  $J_c^{\text{PERC}}(5\text{ K}) = 6.4 \times 10^6\text{ A/cm}^2$  confirming the expected ratio  $J_c^{\text{PERC}}/J_c^G \sim 0.25$ . By assuming  $\langle 2a \rangle \sim 220\ \mu\text{m}$  and evaluating  $J_c^G$  from Eqs. (1), we have also obtained a  $J_c^G$  value which is about half the  $J_c$  of the unpatterned sample, a quite good agreement taking into account that some of the assumptions in the model are no longer fully verified. For example, the trapped field should homogeneously return

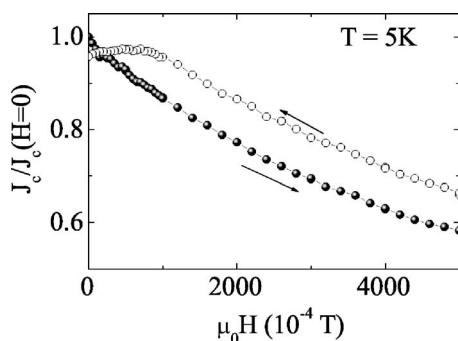


FIG. 5. Magnetic field dependence of the transport critical current density of a porous TFA-YBCO film. Sample was zero-field cooled down to 5 K and  $J_c$  was subsequently measured in increasing field (closed symbols) and in decreasing field (open symbols).

through a single punctual grain boundary instead of an extended array of holes and constrictions, where the mutual inductance between grains should have also been considered. In spite of these difficulties, we can conclude that the experimental result of Fig. 4 confirms our hypothesis and it proves that porosity can lead to unexpected granularity just by geometrical effects in agreement with previous findings.<sup>19–21</sup>

As a final experimental verification we have investigated if these porosity-induced granularity effects can also be seen in transport measurements. For that we have performed transport critical current loops in a porous TFA-YBCO thin film. The following procedure was used: The sample was zero-field cooled down to 5 K and then  $J_c$  was determined as a function of increasing applied field up to 9 T. After, magnetic field was decreased progressively down to zero and the reversal branch of the  $J_c$  loop was thus obtained. The results are shown in Fig. 5. An evident hysteretic behavior is present between the increasing field branch (closed symbols) and the decreasing field branch (open symbols). Moreover, in the reversal branch we can observe the appearance of a peak in the  $J_c$  at positive fields ( $\mu_0 H_{\text{peak}} \sim 0.05$  T) similar to that observed in inductive measurements. These are typical features of granular behavior in transport measurements.<sup>30</sup> Fur-

ther experiments also revealed that peak position and hysteresis are reduced with increasing temperature in agreement with the evolution of the inductive peak. Thus we can affirm that porosity also leads to a granular behavior in transport measurements in epitaxial TFA-YBCO thin films.

In conclusion, we have presented a detailed study of magnetic granularity behavior in YBCO thin films grown by the *ex situ* trifluoroacetates route. This effect has been evidenced by the shift to positive fields of the maximum magnetization in magnetic hysteresis loops. We have demonstrated that this effect is due to the presence of residual porosity in the samples through a mechanism where the holes form a network of constrictions with reduced capability to carry current. In this way the sample behaves as a granular system with two critical current densities, a local  $J_c^G$  and a percolative  $J_c^{\text{PERC}}$ . The analysis of the evolution of this peak in minor hysteresis loops has allowed us to study both  $J_c^G$  and  $J_c^{\text{PERC}}$  for a series of films with different degrees of porosity. We have shown that  $J_c^G$  is almost independent of porosity and indeed it reflects the intrinsic local critical current density of the sample. On the other hand,  $J_c^{\text{PERC}}$  is strongly controlled by porosity and their correlation with normal state resistivity has been proved. In order to prove the geometrical origin of this magnetic granularity, we have fabricated a sample with artificial porosity that forms a bidimensional array of square grains separated by holes and constrictions. We have shown that such sample behaves as a granular system even in absence of low-angle grain boundaries and exhibits the same magnetic behavior as above. The importance of this granularity is evidenced by the hysteretic behavior of the transport critical current.

This work has been supported by the EU (SOLSULET and HIPERCHEM projects), the Spanish CICYT (MAT03-01584 and MAT05-02047), and by the Generalitat de Catalunya (CeRMAE and 2005-SGR-00029). We thank M. Varela for help in preparing the PLD-YBCO thin film. A.P. and J.G. acknowledge Spanish MEC from financial support through Ramón y Cajal and FPU programs, respectively.

\*Present address: Department of Materials Science and Metallurgy, University of Cambridge, Pembroke Street, Cambridge CB2 3QZ, UK.

<sup>1</sup>D. M. Feldmann, J. L. Reeves, A. A. Polyanskii, G. Kozlowski, R. R. Biggers, R. M. Nekkanti, I. Maartense, M. Tomsic, P. Barnes, C. E. Oberly, T. L. Peterson, S. E. Babcock, and D. C. Larbalestier, *Appl. Phys. Lett.* **77**, 2906 (2000).

<sup>2</sup>C. Jooss, L. O. Kautschor, M. P. Delamare, B. Bringmann, K. Guth, V. Born, S. Sievers, H. Walter, J. Dzick, J. Hoffmann, H. C. Freyhardt, B. De Boer, B. Holzappel, and F. Sandiumenge, *Mater. Res. Soc. Symp. Proc.* **659**, II.7.1.1 (2001).

<sup>3</sup>M. A. Angadi, A. D. Caplin, J. R. Laverty, and Z. X. Shen, *Physica C* **177**, 479 (1991).

<sup>4</sup>K. H. Muller, C. Andrikidis, H. K. Liu, and S. X. Dou, *Phys. Rev. B* **50**, 10218 (1994).

<sup>5</sup>S. Tonies, A. Vostner, and H. W. Weber, *J. Appl. Phys.* **92**, 2628

(2002).

<sup>6</sup>D. M. Feldmann, D. C. Larbalestier, D. T. Verebelyi, W. Zhang, Q. Li, G. N. Riley, R. Feenstra, A. Goyal, D. F. Lee, M. Paranthaman, D. M. Kroeger, and D. K. Christen, *Appl. Phys. Lett.* **79**, 3998 (2001).

<sup>7</sup>B. Holzappel, L. Fernandez, F. Schindler, B. de Boer, N. Reger, J. Eickemeyer, P. Berberich, and W. Prusseit, *IEEE Trans. Appl. Supercond.* **11**, 3872 (2001).

<sup>8</sup>A. Palau, T. Puig, X. Obradors, E. Pardo, C. Navau, A. Sanchez, A. Usoskin, H. C. Freyhardt, L. Fernandez, B. Holzappel, and R. Feenstra, *Appl. Phys. Lett.* **84**, 230 (2004).

<sup>9</sup>A. Palau, T. Puig, X. Obradors, R. Feenstra, and H. C. Freyhardt, *IEEE Trans. Appl. Supercond.* **15**, 2790 (2005).

<sup>10</sup>A. Palau, T. Puig, X. Obradors, R. Feenstra, and A. A. Gapud, *Appl. Phys. Lett.* **88**, 122502 (2006).

<sup>11</sup>A. Palau, T. Puig, X. Obradors, R. Feenstra, A. A. Gapud, E. D.

- Specht, D. M. Feldmann, and T. G. Holesinger, *Appl. Phys. Lett.* **88**, 132508 (2006).
- <sup>12</sup>M. W. Rupich, D. T. Verebelyi, W. Zhang, T. Kodenkandath, and X. Li, *MRS Bull.* **29**, 572 (2004).
- <sup>13</sup>X. Obradors, T. Puig, A. Pomar, F. Sandiumenge, N. Mestres, M. Coll, A. Cavallaro, N. Romà, J. Gazquez, J. C. Gonzalez, O. Castaño, J. Gutiérrez, A. Palau, K. Zalamova, S. Morlens, A. Hassini, M. Gibert, S. Ricart, J. M. Moretó, S. Piñol, D. Isfort, and J. Bock, *Supercond. Sci. Technol.* **19**, S1 (2006).
- <sup>14</sup>J. S. Matsuda, Y. Tokunaga, R. Teranishi, H. Fuji, A. Kaneko, S. Asada, T. Honjo, A. Yajima, Y. Iijima, T. Saitoh, T. Izumi, and Y. Shiohara, *Physica C* **412-14**, 890 (2004).
- <sup>15</sup>M. W. Rupich, W. Zhang, X. Li, T. Kodenkandath, D. T. Verebelyi, U. Schoop, C. Thieme, M. Teplitsky, J. Lynch, N. Nguyen, E. Siegal, J. Scudiere, V. Maroni, K. Venkataraman, D. Miller, and T. G. Holesinger, *Physica C* **412-414**, 877 (2004).
- <sup>16</sup>T. Puig, J. C. Gonzalez, A. Pomar, N. Mestres, O. Castaño, M. Coll, J. Gazquez, F. Sandiumenge, S. Piñol, and X. Obradors, *Supercond. Sci. Technol.* **18**, 1141 (2005).
- <sup>17</sup>O. Castaño, A. Cavallaro, A. Palau, J. C. Gonzalez, M. D. Rossell, T. Puig, S. Piñol, N. Mestres, F. Sandiumenge, A. Pomar, and X. Obradors, *IEEE Trans. Appl. Supercond.* **13**, 2504 (2003).
- <sup>18</sup>X. Obradors, T. Puig, A. Pomar, F. Sandiumenge, S. Piñol, N. Mestres, O. Castaño, M. Coll, A. Cavallaro, A. Palau, J. Gázquez, J. Gutiérrez, N. Romà, S. Ricart, J. M. Moretó, M. Rossell, and G. van Tendeloo, *Supercond. Sci. Technol.* **17**, 1055 (2004).
- <sup>19</sup>M. R. Koblischka, L. Pust, A. Galkin, P. Nalevka, M. Jirsa, T. H. Johansen, H. Bratsberg, B. Nilsson, and T. Claeson, *Phys. Rev. B* **59**, 12114 (1999).
- <sup>20</sup>D. V. Shantsev, M. R. Koblischka, Y. M. Galperin, T. H. Johansen, L. Pust, and M. Jirsa, *Phys. Rev. Lett.* **82**, 2947 (1999).
- <sup>21</sup>T. H. Johansen, D. V. Shantsev, M. R. Koblischka, Y. M. Galperin, P. Nalevka, and M. Jirsa, *Physica C* **341**, 1443 (2000).
- <sup>22</sup>E. Bartolome, X. Granados, T. Puig, X. Obradors, E. S. Reddy, and G. J. Schmitz, *Phys. Rev. B* **70**, 144514 (2004).
- <sup>23</sup>T. Araki and I. Hirabayashi, *Supercond. Sci. Technol.* **16**, R71 (2003).
- <sup>24</sup>P. C. McIntyre, M. J. Cima, and M. F. Ng, *J. Appl. Phys.* **68**, 4183 (1990).
- <sup>25</sup>M. R. Koblischka, L. Pust, M. Jirsa, and T. H. Johansen, *Physica C* **320**, 101 (1999).
- <sup>26</sup>K. H. Muller, C. Andrikidis, and Y. C. Guo, *Phys. Rev. B* **55**, 630 (1997).
- <sup>27</sup>H. Hilgenkamp and J. Mannhart, *Rev. Mod. Phys.* **74**, 485 (2002).
- <sup>28</sup>E. J. Garboczi, M. F. Thorpe, M. S. DeVries, and A. R. Day, *Phys. Rev. A* **43**, 6473 (1991).
- <sup>29</sup>E. Bartolome, F. Gomory, X. Granados, T. Puig, and X. Obradors, *Supercond. Sci. Technol.* **18**, 388 (2005).
- <sup>30</sup>J. E. Evetts and B. A. Glowacki, *Cryogenics* **28**, 641 (1988).